Propagation of the equilibrium electron beam in a free-electron laser with an axial guide magnetic field

Shi-Chang Zhang[1,2] and John Elgin[3]
[1]*CCAST (World Laboratory), P.O. Box 8730, Beijing 100080, China*
[2]*Department of Applied Physics, Southwest Jiaotong University, Chengdu, Sichuan 610031, China**
[3]*Department of Mathematics, Imperial College, 180 Queen's Gate, London SW7 2BZ, United Kingdom*
(Received 21 December 1995)

The propagation of the equilibrium electrons in a free-electron laser is analyzed and simulated in various field configurations of the combined wiggler with an axial guide field. It is analytically proven that a reversed guide field may provide a better propagation quality for an electron beam than a positive guide field, which partly gives a theoretical understanding of the efficiency enhancement in the MIT free-electron laser experiment with a reversed guide field [Phys. Rev. Lett. **67**, 3082 (1991)]. Our simulation not only confirms the earlier conclusion that at antiresonance in the uniformly-reversed-field regime the electrons on or near the outer edge of the electron beam may execute highly irregular trajectories and may obtain sufficiently large transverse velocity to be intercepted by the waveguide wall, but also reveals the phenomenon that some electrons close to the axis of the electron beam may obtain sufficiently large transverse velocity to hit the wall before the exit of the wiggler. Nonlinear simulations demonstrate a significant result that the combination of a down-tapered wiggler plus an up-tapered reverse guide field may most effectively improve the propagation quality of the electron beam. [S1063-651X(97)15203-5]

PACS number(s): 41.60.Cr, 52.75.Ms, 41.85.Ja

I. INTRODUCTION

In a free-electron laser (FEL) the propagation quality of the equilibrium electrons affects the gain, operating frequency, and interaction efficiency. An axial magnetic field is often employed to guide the propagation of the electron beam through the wiggler, and to enhance the gain. As is well known, the electrons will get a component of Larmor motion when an axial guide magnetic field $B_0\hat{\mathbf{e}}_z$ is applied. There have been many articles in the literature devoted to the dynamics of the electrons in a combined wiggler with axial guide magnetic fields. As an ideal case, the axis-centered helical orbit and its stability were studied by means of a one-dimensional wiggler model [1–3] and a three-dimensional wiggler model [4–6]. The chaotic features of this ideal helical orbit have been investigated by several authors [7–14]. We constructed the Poincare surface-of-section maps [10,13] and calculated the entropy-like quantity [15] of the relativistic electron in the case of a reversed guide field, and more recently Tsui [16] revealed a new reverse guide field singularity, which partly provided an explanation of the efficiency enhancement observed in a recent FEL experiment with a reversed guide field [17].

In practice, an electron beam has a large number of electrons with *off-axis* guiding centers when they get their transverse velocity $v_\perp$ in the adiabatic range of the wiggler. Therefore, even if the electron beam has *no initial spread* when it is emitted from the electron gun, electrons will diverge in the velocity space and/or configuration space as they propagate through the helical wiggler, since they feel different values of the three-dimensional wiggler field. This divergence deteriorates the propagation quality of the equilibrium electrons, and certainly affects the performance of a free-electron laser. The dynamical behavior of the electrons with off-axis guiding centers was studied by using simulations [18–20], an average wiggler approach [21,22] where the harmonics of the wiggler field were averaged out, and harmonic expansion [23].

In this paper, we study the propagation of the equilibrium electrons in various field configurations and demonstrate that the propagation quality of an electron beam may be improved most effectively by the combination of a down-tapered wiggler with an up-tapered reversed guide field. We organize this paper as follows. In Sec. II a three-dimensional helical wiggler field is expanded in harmonic series. It is the basis to analyze the off-axis electron's motion. Then both the axial and the transverse velocities of an off-axis electron are derived. Based on the functional relationship between velocity fluctuation and the amplitudes of guide field and wiggler field, proposals are qualitatively deduced to improve the propagation quality of the electron beam. In the present paper the terminology ''velocity fluctuation'' refers to the velocity variation of the electrons drifting through the wiggler, but is not the original velocity spreads that the electron beam carries, which are quantified by the beam emittance. In Sec. III nonlinear simulations and comparisons are provided to various field configurations to verify our proposal. Finally, several conclusions are drawn in Sec. IV.

II. ANALYSIS OF ELECTRON'S MOTION

A. General expansion of three-dimensional helical wiggler

The three-dimensional field of a helical wiggler can be expressed in cylindrical coordinates (R,φ,z) as follows [3]:

*Mailing address.

$$\mathbf{B}_w = 2B_w I_1'(k_w R)\cos(\varphi - k_w z)\hat{\mathbf{e}}_R - 2B_w \frac{I_1(k_w R)}{k_w R} \times \sin(\varphi - k_w z)\hat{\mathbf{e}}_\varphi + 2B_w I_1(k_w R)\sin(\varphi - k_w z)\hat{\mathbf{e}}_z , \tag{1}$$

where $\hat{\mathbf{e}}_R$, $\hat{\mathbf{e}}_\varphi$, and $\hat{\mathbf{e}}_z$ are the basis vectors in cylindrical coordinates, B_w and k_w are the wiggler amplitude and wavenumber (i.e., $k_w = 2\pi/\lambda_w$, λ_w being the length of the wiggler period), and I_n and I_n' are the nth-order modified Bessel function and its derivative with respective to the argument, respectively. In the combination of a helical wiggler with an axial guide magnetic field the dynamic analysis of the electron's motion with off-axis guiding centers may become easy if the helical wiggler field is expanded in terms of the simultaneous cyclotron radius, cyclotron angle, and the guiding-center position. Before we consider the specific physical system, let us first derive the general expansion of Eq. (1) in terms of basis vectors $\hat{\mathbf{e}}_r$ and $\hat{\mathbf{e}}_\theta$ shown in Fig. 1(a). This procedure is a purely mathematical calculation without any physical restrictions. The transformation of basis vector from $(\hat{\mathbf{e}}_R, \hat{\mathbf{e}}_\varphi)$ to $(\hat{\mathbf{e}}_r, \hat{\mathbf{e}}_\theta)$ is

$$\hat{\mathbf{e}}_R = \hat{\mathbf{e}}_r \cos(\varphi - \theta) + \hat{\mathbf{e}}_\theta \sin(\varphi - \theta), \tag{2}$$

$$\hat{\mathbf{e}}_\varphi = -\hat{e}_r \sin(\varphi - \theta) + \hat{\mathbf{e}}_\theta \cos(\varphi - \theta). \tag{3}$$

Then the transverse component of the wiggler field can be rewritten as

$$\mathbf{B}_{w\perp} = \hat{\mathbf{e}}_r B_w [I_0(\overline{R})\cos(\theta - \overline{z}) + I_2(\overline{R})\cos(2\varphi - \theta - \overline{z})] + \hat{\mathbf{e}}_\theta B_w [-I_0(\overline{R})\sin(\theta - \overline{z}) + I_2(\overline{R})\sin(2\varphi - \theta - \overline{z})], \tag{4}$$

where we have normalized R and z as $\overline{R} = k_w R$ and $\overline{z} = k_w z$. With the aid of Graf's addition theorem of modified Bessel function [24] for the triangle ΔOAG (see Fig. 1)

$$I_n(\overline{R})\cos(n\xi) = \sum_{m=-\infty}^{\infty} (-1)^m I_{m+n}(\overline{R_g}) I_m(\overline{r})\cos(m\psi), \tag{5}$$

$$I_n(\overline{R})\sin(n\xi) = \sum_{m=-\infty}^{\infty} (-1)^m I_{m+n}(\overline{R_g}) I_m(\overline{r})\sin(m\psi), \tag{6}$$

where

$$\xi = \varphi_g - \varphi, \tag{7}$$

$$\psi = (\pi - \varphi_g) + \theta, \tag{8}$$

and $\overline{R_g} = k_w R_g$, we obtain the general expansion of helical wiggler field as follows:

$$\mathbf{B}_{w\perp} = -\hat{\mathbf{e}}_r B_w \sum_{l=-\infty}^{\infty} I_l(\overline{R_g}) I_l(\overline{r})\cos[l(\theta - \varphi_g)]\cos(\theta - \overline{z}) + \hat{\mathbf{e}}_r B_w \sum_{l=-\infty}^{\infty} I_{l+2}(\overline{R_g}) I_l(\overline{r})\cos[2\varphi_g - l(\theta - \varphi_g) - (\theta + \overline{z})]$$
$$- \hat{\mathbf{e}}_\theta B_w \sum_{l=-\infty}^{\infty} I_l(\overline{R_g}) I_l(\overline{r})\cos[l(\theta - \varphi_g)]\sin(\theta - \overline{z}) + \hat{\mathbf{e}}_\theta B_w \sum_{l=-\infty}^{\infty} I_{l+2}(\overline{R_g}) I_l(\overline{r})\sin[2\varphi_g - l(\theta - \varphi_g) - (\theta + \overline{z})], \tag{9}$$

$$\mathbf{B}_{wz} = 2B_w \sum_{l=-\infty}^{\infty} I_{l-1}(\overline{R_g}) I_l(\overline{r})\sin[l(\theta - \varphi_g) + \varphi_g - \overline{z}]\hat{\mathbf{e}}_z . \tag{10}$$

It should be emphasized that R_g and φ_g are restricted by the geometrical relationship

$$R_g = [R^2 + r^2 - 2Rr\cos(\theta - \varphi)]^{1/2}, \tag{11}$$

$$\varphi_g = \arctan\left[\frac{R\sin(\varphi) - r\sin(\theta)}{R\cos(\varphi) - r\cos(\theta)}\right], \tag{12}$$

or by the relationship

$$R_g\cos(\varphi_g) = R\cos(\varphi) - r\cos(\theta), \tag{13}$$

$$R_g\sin(\varphi_g) = R\sin(\varphi) - r\sin(\theta). \tag{14}$$

Now we examine the physical meaning of Eqs. (9) and (10). Suppose that in Fig. 1(a) point A denotes the simultaneous location of the considered electron, and point G is its guiding center. Then Eqs. (9) and (10) indicate that from the point of view of the considered electron, the wiggler field turns out to be a series of cyclotron harmonics about the cyclotron angle θ. Generally speaking, the local field felt by the electron is related with both the rotating motion around the guiding center and the guiding-center shift, that is, related with the simultaneous Larmor radius r, cyclotron angle θ, and the guiding-center position R_g and φ_g.

B. Specific expansion on a helical orbit

The expansion of the wiggler field on a helical orbit can be easily derived from Eqs. (9) and (10). In the combined wiggler with an axial guide magnetic field, the helical orbit has the property of $\theta - \overline{z} = \pi/2$ for group I orbits and $\theta - \overline{z} = -\pi/2$ for group II orbits and $\overline{z} = k_w v_\parallel t$ [1–6]. Substituting this relationship into Eqs. (9) and (10), and, without loss of generality, letting $\varphi_g = \pi/2$, one can obtain the expansion of the wiggler on a helical orbit

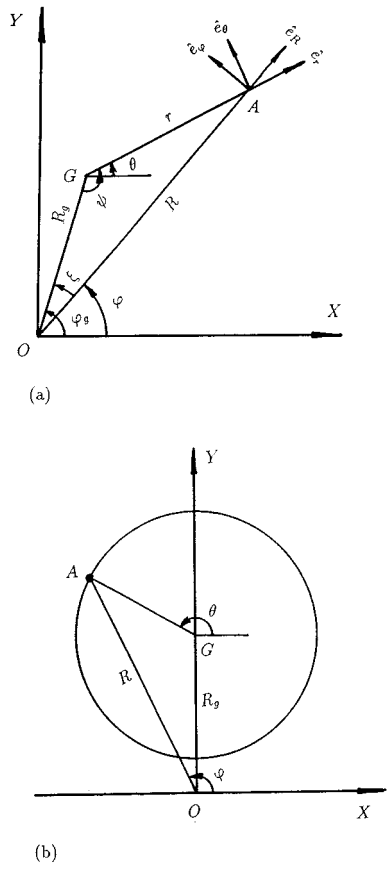

FIG. 1. Coordinate systems employed in the harmonic expansion of a helical wiggler field in (a) general case, and (b) specific case of a helical orbit.

$$\mathbf{B}_{w\perp}=\hat{\mathbf{e}}_r B_w \sum_{n=-\infty}^{\infty} I_n(\overline{R_g}) I_{n-2}(\overline{r})\sin(n\overline{z}) + \hat{\mathbf{e}}_\theta B_w \sum_{n=-\infty}^{\infty} \frac{2(n-1)}{\overline{r}} I_n(\overline{R_g}) I_{n-1}(\overline{r})\cos(n\overline{z}), \tag{15}$$

and

$$\mathbf{B}_{wz}=2B_w \sum_{n=-\infty}^{\infty} I_n(\overline{R_g}) I_{n+1}(\overline{r})\cos(n\overline{z})\hat{\mathbf{e}}_z . \tag{16}$$

If one averages Eqs. (15) and (16) within a cyclotron period, that is, integrates with respect to z over a wiggler period λ_w, one obtains

$$\langle \mathbf{B}_{w\perp} \rangle = -2B_w \frac{I_1(\overline{r})}{\overline{r}} I_0(\overline{R_g})\hat{\mathbf{e}}_\theta , \tag{17}$$

$$\langle \mathbf{B}_{wz} \rangle = 2B_w I_1(\overline{r}) I_0(\overline{R_g})\hat{\mathbf{e}}_z , \tag{18}$$

which coincides with the expressions given in Ref. [21]. Here we see that $\langle \mathbf{B}_{w\perp} \rangle$ and $\langle \mathbf{B}_{wz} \rangle$ turn out to be the lowest approximation in Eqs. (15) and (16), that is, the only one harmonic with $n=0$ in Eqs. (15) and (16). It will be useful to rewrite Eqs. (15) and (17) in Cartesian coordinates [cf. Fig. 1(b)] as

$$\mathbf{B}_{w\perp}=2B_w \sum_{n=-\infty}^{\infty} \frac{n}{\overline{r}} I_n(\overline{r}) I_{n-1}(\overline{R_g}) \times [\hat{\mathbf{e}}_x \cos(nk_w \overline{v_\parallel} t)+\hat{\mathbf{e}}_y \sin(nk_w \overline{v_\parallel} t)], \tag{19}$$

$$\langle \mathbf{B}_{w\perp} \rangle = 2B_w \frac{I_1(\overline{r})}{\overline{r}} I_0(\overline{R_g})[\hat{\mathbf{e}}_x \cos(k_w \overline{v_\parallel} t)+\hat{\mathbf{e}}_y \sin(k_w \overline{v_\parallel} t)], \tag{20}$$

where $\hat{\mathbf{e}}_x$ and $\hat{\mathbf{e}}_y$ are the unit vectors in x and y directions, respectively.

C. Analysis of electron's velocity

It is difficult to derive the *exact* solution of the equation of motion for a relativistic electron with off-axis guiding center in a combined helical wiggler with axial guide magnetic field. As a matter of fact, we have shown that there is no purely helical orbit as the guiding center is off axis [22]. In order to give prominence to the effect of the velocity harmonics, we approximately evaluate the magnetic forces on an ideal helical orbit with equivalent Larmor radius $\overline{r}$ and equivalent guiding-center position R_g.

The equation of the transverse motion may be approximately expressed by

$$\frac{d(\gamma m_0 \mathbf{v}_\perp)}{dt} = -e[\mathbf{v}_\perp \times (B_0 \hat{\mathbf{e}}_z + \langle \mathbf{B}_{wz} \rangle) + \overline{v_\parallel}\hat{\mathbf{e}}_z \times \mathbf{B}_{w\perp}], \tag{21}$$

where γ, m_0, $-e$, $\mathbf{v}_\perp$, and $\overline{v_\parallel}$ are the electron's relativistic energy factor, rest mass, negative charge, transverse velocity, and the average of the axial velocity, respectively. Substituting Eqs. (18) and (19) into (21) yields

$$\mathbf{v}_\perp = v_{\perp 0}[\cos(\overline{\Omega_\parallel} t+\varphi_0)\hat{\mathbf{e}}_x + \sin(\overline{\Omega_\parallel} t+\varphi_0)\hat{\mathbf{e}}_y] + \mathbf{v}_{\perp,\mathrm{fluc}}, \tag{22}$$

where

$$\mathbf{v}_{\perp,\mathrm{fluc}} = -\sum_{n=1}^{\infty} [\hat{\mathbf{e}}_x v_{xn} \cos(nk_w \overline{v_\parallel} t)+\hat{\mathbf{e}}_y v_{yn} \sin(nk_w \overline{v_\parallel} t)], \tag{23}$$

and the amplitudes v_{xn} and v_{yn} are

$$v_{xn}=\frac{4n^2 \Omega_w \overline{v_\parallel} I_n(\overline{r})}{\overline{r}(nk_w \overline{v_\parallel}-\overline{\Omega_\parallel})(nk_w \overline{v_\parallel}+\overline{\Omega_\parallel})} \times [k_w \overline{v_\parallel} I_n'(\overline{R_g})+\overline{\Omega_\parallel} I_n(\overline{R_g})/\overline{R_g}], \tag{24}$$

$$v_{yn}=\frac{4n\Omega_w \overline{v_\parallel} I_n(\overline{r})}{\overline{r}(nk_w \overline{v_\parallel}-\overline{\Omega_\parallel})(nk_w \overline{v_\parallel}+\overline{\Omega_\parallel})} \times [n^2 k_w \overline{v_\parallel} I_n(\overline{R_g})/\overline{R_g}+\overline{\Omega_\parallel} I_n'(\overline{R_g})]. \tag{25}$$

Here $\overline{\Omega_\parallel}=e[B_0+2B_w I_1(\overline{r}) I_0(\overline{R_g})]/(\gamma m_0 c)$, $\Omega_w = eB_w/(\gamma m_0 c)$, c is the light speed in vacuum, B_0 is the amplitude of the axial guide field, and $v_{\perp 0}$ and φ_0 are the integral constants, which depend on the entrance condition, respectively.

The equation of axial motion may be approximately determined by

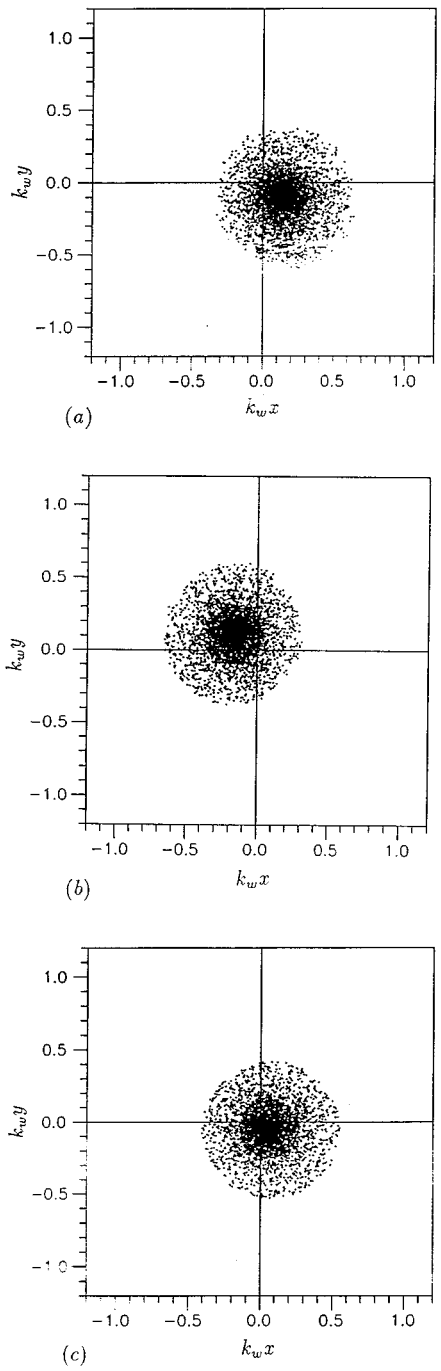

FIG. 2. Cross-sectional views of the 5000 test electrons at the exit of the wiggler for (a) group I with $B_0=4.06$ kG, $B_{w0}=0.63$ kG, $I_b=90$ A, (b) group II with $B_0=10.9$ kG, $B_{w0}=0.63$ kG, $I_b=300$ A, and (c) reversed guide field with $B_0=-10.9$ kG, $B_{w0}=1.47$ kG, $I_b=300$ A, where the initial state of these 5000 test electrons is the Gaussian random distribution. Herein and hereafter the relativistic energy factor of the beam is 2.4677 with an initial Gaussian spread of 1%, the average radius of the beam is 0.25 cm, the wiggler period is 3.18 cm, the wiggler length is 2 m, the adiabatic range has a length of six wiggler periods, and the drift tube is a cylindrical waveguide with a radius of 0.51 cm.

$$\frac{d\mathbf{v}_z}{dt}=-\frac{e}{\gamma m_0 c}\,\mathbf{v}_\perp\times\langle\mathbf{B}_{w\perp}\rangle. \tag{26}$$

Inserting Eqs. (20) and (22) into (26), we obtain

$$v_z=v_{z0}+v_{z,\mathrm{fluc}}, \tag{27}$$

$$v_{z,\mathrm{fluc}}=\sum_{n=1}^{\infty} v_{zn}\cos(nk_w\overline{v_\parallel}t), \tag{28}$$

where the amplitude v_{zn} is

$$v_{zn}=\frac{4\Omega_w^2 I_1(\overline{r})I_0(\overline{R_g})I_n(\overline{R_g})}{nk_w\overline{r^2}} \times\left[\frac{(n+1)I_{n+1}(\overline{r})}{(n+1)k_w\overline{v_\parallel}-\overline{\Omega_\parallel}}-\frac{(n-1)I_{n-1}(\overline{r})}{(n-1)k_w\overline{v_\parallel}+\overline{\Omega_\parallel}}\right], \tag{29}$$

and v_{z0} is the integral constant, which depends on the entrance condition.

D. Improvement of the beam's propagation quality

The first terms in Eqs. (22) and (27) denote the initial velocities on a helical orbit, which depend on the entrance conditions, while the second terms in Eqs. (22) and (27) represent fluctuation velocities relative to the initial velocities $v_{\perp 0}$ and v_{z0}. As the off-axis-guiding-center electrons have different R_g and $\overline{r}$, the values of their v_{xn}, v_{yn}, and v_{zn} must be different. An *electron beam* in the combined wiggler with axial guide magnetic field has a large number of off-axis electrons with different distances from the axis, i.e., with different Larmor radii and guiding centers. Therefore, the divergence of the electron beam in velocity space is inevitable when the electron beam propagates through the wiggler, no matter how small the initial velocity spread is. Noting that both the magnetostatic wiggler field and axial guide magnetic field do no work, and that the electron's energy maintains its initial value at entrance $[1-(v_{\perp 0}^2+v_{z0}^2)/c^2]^{-1/2}$ when the electron beam propagates through the wiggler, we understand that a relatively small fluctuation of transverse velocity corresponds to a relatively small fluctuation of axial velocity, and vice versa. Evidently, in order to improve the propagation quality of an electron beam, it is essential to suppress the velocity fluctuations v_{zn} and $v_{\perp n}$ of the electrons.

In Eqs. (24) and (25), $I_n(\overline{R_g})>0$ and $I_n'(\overline{R_g})>0$ hold, thus in the case of a reversed guide field ($\Omega_\parallel<0$) the numerator is smaller than that in a positive guide field ($\Omega_\parallel>0$). For example, at resonance ($|\overline{\Omega_\parallel}|\approx k_w\overline{v_\parallel}$) v_{xn} and v_{yn} are approximately proportional to $I_2(R_g)$ in a reversed guide field, while v_{xn} and v_{yn} are approximately proportional to $I_0(R_g)$ in a positive guide field. Therefore, we draw an important conclusion that a reversed guide field ($\Omega_\parallel<0$) may provide a better propagation quality for the electron beam than a positive guide field ($\Omega_\parallel>0$). This conclusion may partly give a theoretical understanding of the efficiency enhancement in the recent FEL experiment in MIT where the positive guide field was replaced by a reversed guide field [17].

From the physical and mathematical points of view, we may dissociate a tapered field slightly varying with the axial distance as many discrete statuses, each of which corresponds to a situation of a constant field, and then analyze one

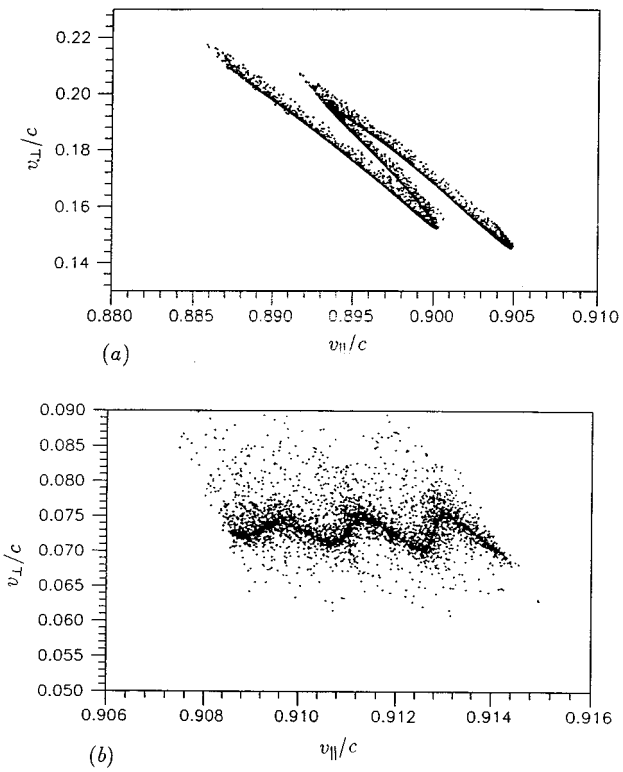

FIG. 3. Velocity distributions of the 5000 test electrons at the exit of the wiggler for (a) group I, and (b) reversed guide field, where the parameters are the same as those in Fig. 2.

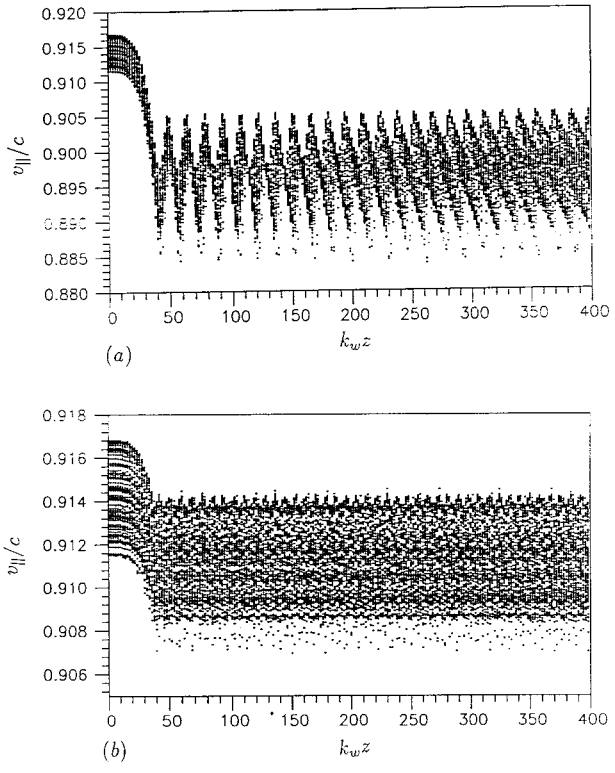

FIG. 4. Evolutions of the normalized axial velocity versus the axial distance for (a) group I, and (b) reversed guide field, where 100 electrons are plotted which are selected *at random* from the 5000 test electrons, and parameters are the same as those in Fig. 2.

after another. Although the above formulas are derived in a untapered field and cannot reflect the *exact* behavior of an electron in a tapered field, we may *qualitatively* deduce the *tend* of the velocity fluctuation of the electron beam in tapered field by investigating the functional relationship in the above formulas. It is easy to show that in Eq. (29) v_{zn} is an increasing function of wiggler field, and also is an increasing function of $\Omega_\parallel$ in a positive guide field, but is a decreasing function of $|\Omega_\parallel|$ in a reversed guide field. Therefore, a down-tapered positive guide field seems to be better than an untapered positive guide field, and an up-tapered reversed guide field is better than the uniformly reversed guide field. Considering the functional relationship mentioned above, we propose a combined field configuration of a down-tapered wiggler with an up-tapered reversed guide field, which may most effectively improve the propagation quality of the electron beam. In the following section we shall present detailed simulations of propagation of the electron beam to verify this proposal.

III. NONLINEAR SIMULATIONS OF *E*-BEAM PROPAGATION

In order to demonstrate the advantage of the field combination of a down-tapered wiggler plus an up-tapered reversed guide field, we give comparisons by simulating the propagation of the electron beam in various field configurations. In the nonlinear simulations, we assume that the initial states of the tested electrons in velocity space and configuration space are a Gaussian *random* distribution, and we trace 5000 test electrons with initial energy spread $\Delta\gamma_{z0}/\gamma_0=1\%$. Each test

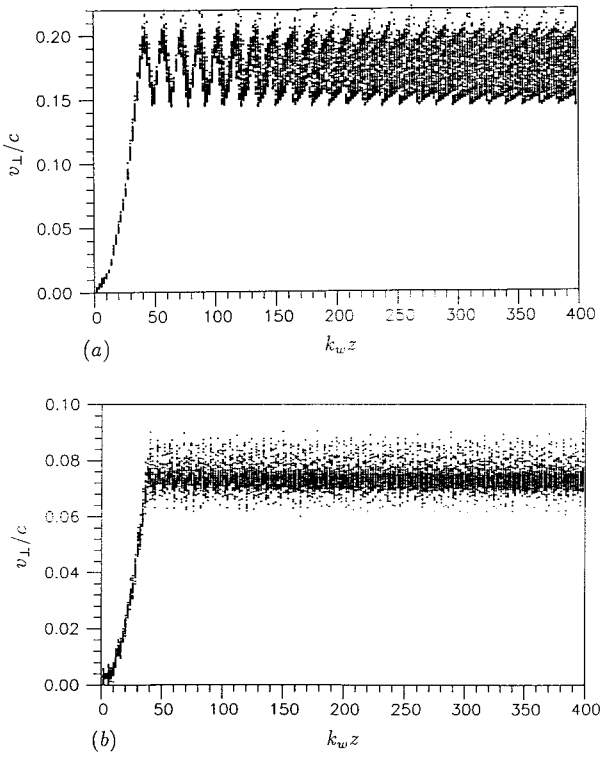

FIG. 5. Evolutions of the normalized transverse velocity vs the axial distance for (a) group I and (b) reversed guide field, where 100 electrons are plotted, which are selected *at random* from the 5000 test electrons, and parameters are the same as those in Fig. 2.

electron is governed by the equation of motion

$$\frac{d(\gamma m_0 \mathbf{v})}{dt} = -e[\mathbf{E}_s + \mathbf{v}\times(\mathbf{B}_w + \mathbf{B}_g + \mathbf{B}_s)]. \tag{30}$$

Here $\mathbf{B}_w$ is the wiggler field shown in Eq. (1) with $B_w = B_{w0}[1+\zeta(\overline{z}-\overline{z}_{w0})]$ where the amplitude of the wiggler is tapered with slope ζ at the position $\overline{z}_{w0}$, the axial guide field is tapered with slope ϵ at $\overline{z}_{g0}$,

$$\mathbf{B}_g = B_0[1+\epsilon(\overline{z}-\overline{z}_0)]\hat{\mathbf{e}}_z - \tfrac{1}{2}\epsilon B_0(\overline{x}\hat{\mathbf{e}}_x + \overline{y}\hat{\mathbf{e}}_y), \tag{31}$$

and $\mathbf{E}_s$ and $\mathbf{B}_s$ are the self-fields of the electron beam [25]:

$$\mathbf{E}_s = -(m_0/2e)R\omega_b^2\hat{\mathbf{e}}_R, \tag{32}$$

$$\mathbf{B}_s = -[(m_0/2e)v_{z0}R\omega_b^2\hat{\mathbf{e}}_\varphi, \tag{33}$$

where ω_b is the plasma frequency of the electron beam, and $\overline{z}=k_w z$ is the normalized quantity of z. The equation of motion is solved in terms of the Runge-Kutta method of order four, and the invariant $\gamma[1-(v/c)^2]^{1/2}$ is chosen to monitor the accuracy of the iterations. In the simulation we choose the typical parameters of the MIT experiment as follows [17]: the relativistic energy factor is 2.4677, the average radius of the electron beam is 0.25 cm, the drift tube is a cylindrical waveguide with radius of 0.51 cm, the wiggler period is 3.18 cm, the wiggler length is about 2 m, and the adiabatic range of the wiggler has a length of six wiggler periods. The profile function of the magnetic field in the adiabatic range that is included in our numerical analysis results from our simulation of the reported measurements of the MIT experimental facility (cf. Fig. 4 in Ref. [26]).

A. Untapered field configurations

Firstly, we simulate the propagation of the electron beam in untapered wiggler plus an untapered positive guide field or plus an uniformly reversed guide field. Figure 2 shows the cross-sectional views of the 5000 test electrons at the exit of the wiggler for (a) group I with $B_0=4.06$ kG, $B_{w0}=0.63$ kG, $I_b=90$ A, (b) group II with $B_0=10.9$ kG, $B_{w0}=0.63$ kG, $I_b=300$ A, and (c) uniformly reversed field with $B_0=-10.9$ kG, $B_{w0}=1.47$ kG, $I_b=300$ A. Although the electron beam does not diverge in the configuration space for all the three circumstances, the *axis* of the electron beam substantially deviates from the symmetrical axis of the cylindrical waveguide when the guide field is positive. This deviation certainly affects the interaction between the electron beam and the rf fields of the waveguide, because it changes the location of the beam in the waveguide. In the MIT experiment [17], indeed, the efficiency of the beam-wave interaction is 9%, 2%, and 27% for the group I, group II, and reversed field parameters, respectively. Besides the configuration deviation, the velocity fluctuation of the electron beam in the process of propagation through the wiggler may be an important factor to affect the beam-wave interaction. Figure 3 displays the comparison of the velocity distributions of the 5000 test electrons at the exit of the wiggler for the group I and for the uniformly reversed field. It is found that the velocity span in a positive guide field is much wider than the velocity span in the uniformly reversed guide field. To further examine the details of the propagation of the electrons, we plot, in Figs. 4 and 5, the evolutions of the axial velocity and the transverse velocity of 100 electrons which are selected *at random* from the 5000 test electrons. One can see from Figs. 4 and 5 that after the adiabatic range the axial and transverse velocity fluctuations are, respectively, $\Delta v_\parallel/c\approx 0.02$ and $\Delta v_\perp/c\approx 0.08$ in the case of the positive guide field, while in the case of the uniformly reversed guide field the axial and transverse velocity fluctuations are $\Delta v_\parallel/c\approx 0.007$ and $\Delta v_\perp/c\approx 0.03$, respectively. These results demonstrate that a positive guide field yields more serious velocity fluctuation than uniformly reversed guide field when the electrons propagate through the wiggler.

In summary, a uniformly reversed guide field may present a better propagation quality for an electron beam than a positive guide field. This conclusion coincides with the result derived in Sec. II.

B. Up-tapered reverse guide field configuration

Although the uniformly reversed field is in favor of the beam propagation compared with a positive guide field, both the MIT experiment [17] and the theoretical analysis [23] as well as Eqs. (24) and (25) in Sec. II indicate that the electron beam diverges at the antiresonance ($B_{w0}=1.47$ kG, $B_0=-7.6$ kG). Now we give a comparison between the propagations of an electron beam in a uniformly reversed guide field and in an up-tapered reversed guide field. Figure 6 gives the details of the evolutions in configurations space and velocity space for 100 electrons, which are selected at random from the 5000 test electrons, where 16 electrons of these 100 electrons hit the wall of the cylindrical waveguide at the positions plotted by the horizontal lines. Figure 8 shows a loss of about 17% of the 5000 test electrons on the waveguide wall, and only 83% of the test electrons pass through the wiggler. Here the simulation is in excellent agreement with the measured data in the MIT experiment where the beam current decreased from 300 A at the entrance of the wiggler to 248 A at the exit of the wiggler. Figures 6(a)–6(d) show a serious deterioration of the propagation quality of the electron beam at anti-resonance, which supports the earlier opinion [19,23] that the output power dip at the antiresonance observed in the MIT experiment [17] results from both the loss of the beam current and the poor propagation quality of the electron beam. It should be pointed out that the previous literatures [19,23] only found that at antiresonance the electrons on or near the outer edge of the beam may execute highly irregular trajectories and may obtain sufficiently large transverse velocity to be intercepted by the wall of the waveguide. As shown in Fig. 6, however, our simulation reveals that the electrons even close by the axis of the beam maybe obtain sufficiently large transverse velocity to hit the wall before the exit of the wiggler, although their orbits are nearly helical.

As we expected in Sec. II, Figs. 7 and 8 indicate a dramatic improvement of the beam propagation at antiresonance by an up tapered reversed guide field at $k_w z_{g0}=40$ with slope $\epsilon=0.01$. No electron hits the wall of the waveguide before the exit of the wiggler, and the divergence of the beam in both configuration space and velocity space becomes small.

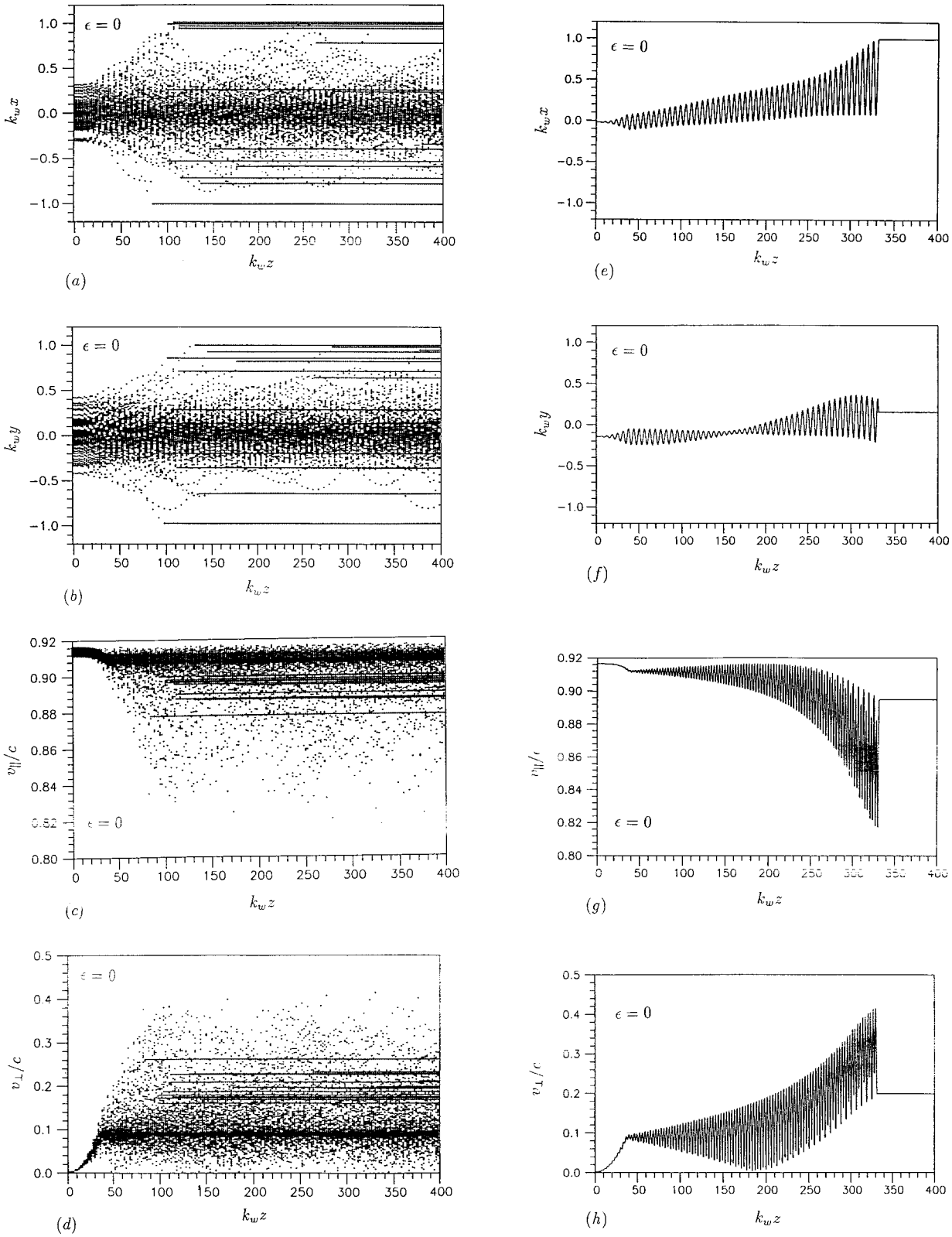

FIG. 6. Evolutions of (a), (b) the normalized transverse position and (c), (d) the normalized velocity vs the axial distance at *antiresonance* with $B_{w0}=1.47$ kG, $I_b=300$ A, and uniformly reversed guide field $B_0=-7.6$ kG, where 100 electrons are selected at random from the 5000 test electrons and plotted; figures (e), (f), (g), and (h) display the evolutions of the normalized transverse position and normalized velocity of an electron, which is close by the axis of the beam.

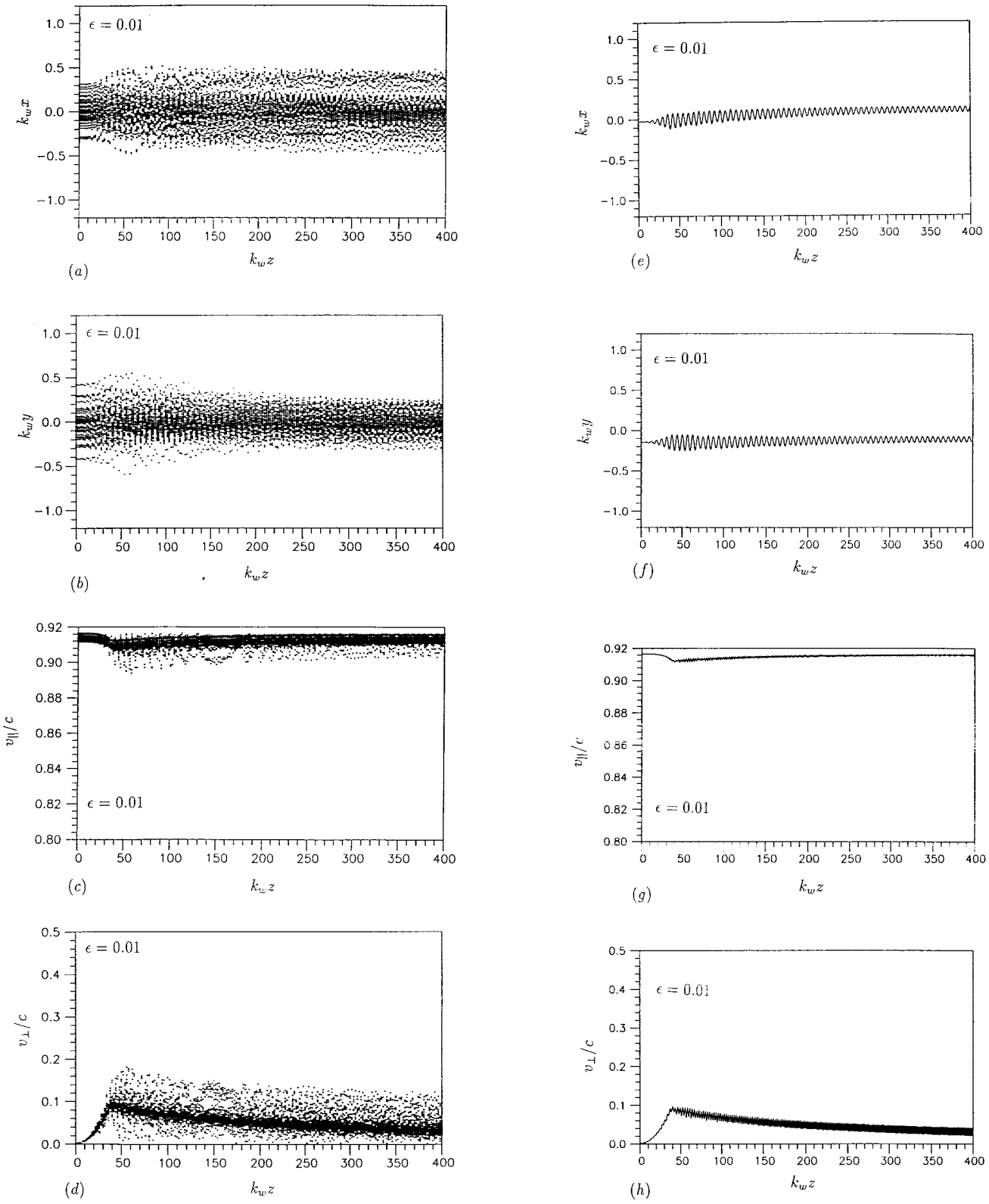

FIG. 7. Evolutions of (a), (b) the normalized transverse position, and (c), (d) the normalized velocity vs the axial distance at *antiresonance* with $B_{w0}=1.47$ kG, $I_b=300$ A, and reversed guide field $B_0=-7.6$ kG up-tapered at $k_w z_{g0}=40$ with slope $\epsilon=0.01$, where 100 electrons are selected at random from the 5000 test electrons and plotted; figures (e), (f), (g), and (h) display the evolutions of the normalized transverse position and normalized velocity of the electron corresponding to the one in Figs. 6(e), (f), (g), and (h).

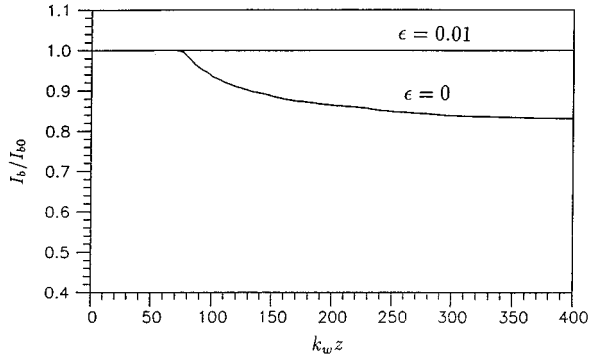

FIG. 8. Comparison of the beam loss at antiresonance between an untapered reversed guide field ($\epsilon=0$) and a reversed guide field up-tapered at $k_w z_{g0}=40$ with slope $\epsilon=0.01$, where I_{b0} denotes the value of the beam current at the entrance of the wiggler. The loss of 17% of the beam current when $\epsilon=0$ is in excellent agreement with the observation in the MIT experiment [17].

The above comparison demonstrates that an up-tapered reversed guide field may provide a better propagation quality for an electron beam than a uniformly reversed guide field. The qualitative deduction in Sec. II is in agreement with this nonlinear result.

C. Combination of a down-tapered wiggler with an up-tapered reversed guide field

In a free-electron laser the self-fields of the electron beam plays an important role if the beam current is high. For example, the self-fields of the electron beam may cause a new kind of unstable orbit [6], induce chaotic behavior [7,10], generate a new reverse guide field singularity [16], affect the dispersion property of the waveguide modes [27], and tend to reduce saturation efficiency and enhance beam spreading depending upon the magnitude of the external beam focusing [28]. In this subsection an electron beam with a high current $I_b=2000$ A is considered. Figure 9 provides comparisons of the velocity distribution at the exit of the wiggler at nonresonance with $B_{w0}=1.47$ kG, $B_0=-10.9$ kG for (a) untapered fields ($\zeta=0$, $\epsilon=0$), (b) untapered wiggler ($\zeta=0$) plus a reversed guide field up-tapered at $k_w z_{g0}=40$ with $\epsilon=0.0012$, and (c) a wiggler down-tapered with $\zeta=-0.0018$ plus a reversed guide field up-tapered with $\epsilon=0.0012$, both beginning at $k_w z=40$. The results shown in Fig. 9(a) and 9(b) confirm the conclusion obtained at antiresonance in the last subsection: The propagation quality of the electron beam in up-tapered reversed guide field is better than in uniformly reversed guide field. More importantly, it is demonstrated in Fig. 9 that the combined configuration of a down-tapered wiggler with an up-tapered reversed guide field may be the most effective approach to improve the propagation quality of the electron beam.

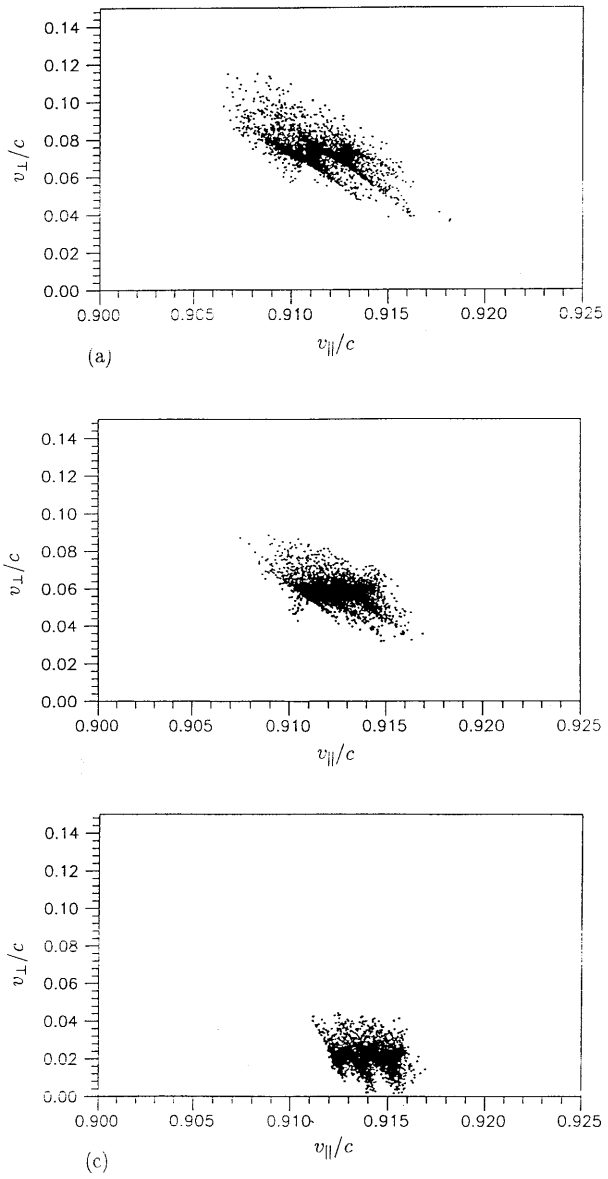

FIG. 9. Velocity distributions of the 5000 test electrons at the exit of the wiggler at nonresonance with $B_{w0}=1.47$ kG, $B_0=-10.9$ kG for (a) untapered fields ($\zeta=0$, $\epsilon=0$), (b) untapered wiggler ($\zeta=0$) plus a reversed guide field up-tapered ($\epsilon=0.0012$) at $k_w z_{g0}=40$, and (c) a wiggler down-tapered ($\zeta=-0.0018$) plus a reversed guide field up-tapered ($\epsilon=0.0012$), both beginning at $k_w z=40$, where the beam current is 2000 A, and other parameters are the same as those in Fig. 2.

IV. CONCLUSIONS

In this paper we have presented detailed three-dimensional analysis and nonlinear simulations for the propagation of the electrons in various field configurations, including the circumstance with high beam current. The following conclusions can be drawn.

(1) A uniformly reversed guide field can present a better propagation quality for an electron beam drifting through the wiggler than an untapered positive guide field. Additionally, at antiresonance in the uniformly-reversed-field regime not only the electrons on or near the outer edge of the beam may execute highly irregular trajectories and may obtain sufficiently large transverse velocity to be intercepted by the wall of the waveguide, but also the electrons close to the axis of the beam may obtain sufficiently large velocity to hit the wall before the exit of the wiggler.

(2) The propagation quality of the electron beam in an up-tapered reversed guide field may be better than in a uniformly reversed guide field.

(3) The most effective approach to improve the propagation quality of the electron beam may be the combined configuration of a down-tapered wiggler with an up-tapered reversed guide field.

Based on the above conclusions, a free-electron laser with down-tapered wiggler plus up-tapered reversed guide field is proposed, and further calculation including the radiation fields is undertaken.

ACKNOWLEDGMENTS

This work was supported by the National Natural Science Foundation of China and the UK Royal Society.

[1] L. Frieland, Phys. Fluids **23**, 2376 (1980).
[2] H. P. Freund and A. T. Drobot, Phys. Fluids **25**, 736 (1982).
[3] P. Diament, Phys. Rev. A **23**, 2537 (1981).
[4] H. P. Freund, S. Johnson, and P. Sprangle, IEEE J. Quantum Electron. **19**, 322 (1983).
[5] H. P. Freund and A. K. Ganguly, IEEE J. Quantum Electron. **21**, 1073 (1985).
[6] S. C. Zhang and Z. Zhang, Appl. Phys. Lett. **55**, 1380 (1989).
[7] C. Chen and R. C. Davidson, Phys. Rev. A **42**, 5041 (1990).
[8] G. Spindler and G. Renz, Phys. Fluids B **3**, 3517 (1991).
[9] L. Michel, A. Bourdier, and J. M. Buzzi, Nucl. Instrum. Methods Phys. Res. A **304**, 465 (1991).
[10] S. C. Zhang and Y. Xu, SPIE Proc. **1929**, 64 (1992).
[11] S. C. Zhang, *Introduction to Free-Electron Lasers*, chap. 3, January 1993 (Southwest Jiaotong University Press, Chengdu, 1993).
[12] S. C. Zhang and Y. Xu, Phys. Lett. A **179**, 311 (1993).
[13] S. C. Zhang, Y. Xu, and Q. X. Liu, Phys. Rev. E **48**, 3952 (1993).
[14] A. Bourdier and L. Michel-Lours, Phys. Rev. E **49**, 3353 (1994).
[15] S. C. Zhang, Q. X. Liu, and Y. Xu, Acta Physica Sinica **43**, 225 (1994).
[16] K. H. Tsui, Phys. Plasmas **2**, 3865 (1995).
[17] M. E. Conde and G. Bekefi, Phys. Rev. Lett. **67**, 3082 (1991).
[18] A. Pasaer, F. Mako, and C. W. Roberson, J. Appl. Phys. **53**, 7174 (1982).
[19] H. P. Freund and A. K. Ganguly, IEEE Trans. Plasma Sci. **20**, 245 (1992); also H. P. Freund, Phys. Fluids B **5**, 1869 (1993).
[20] J. Gardelle, J. Labrouche, and P. Le Taillandier, Phys. Rev. E **50**, 4973 (1994).
[21] J. Fajans, D. A. Kirkpatrick, and G. Bekefi, Phys. Rev. A **32**, 3448 (1985).
[22] S. C. Zhang and Z. Zhang, Int. J. Infrared Millimeter Waves **9**, 1107 (1988).
[23] K. R. Chu and A. T. Lin, Phys. Rev. Lett. **67**, 3235 (1991).
[24] G. N. Watson, *Theory of Bessel Functions* (Cambridge University Press, Cambridge, 1952), Chap. XI, pp. 359–361.
[25] H. S. Uhm and R. C. Davidson, Phys. Fluids **29**, 2713 (1986).
[26] J. Fajans, G. Bekefi, Y. Z. Yin, and B. Lax, Phys. Fluids **28**, 1995 (1985).
[27] S. C. Zhang and Z. Zhang, J. Appl. Phys. **66**, 3463 (1989).
[28] H. P. Freund, R. H. Jackson, and D. E. Pershing, Phys. Fluids B **5**, 2318 (1993).